

Oriental Growth of Flexible van der Waals Supramolecular Networks

Ding, Haoxuan; Zhang, Xin; Li, Bosheng; Wang, Yitao; Xia, Chunqiu; Zhao, Haoyu; Yang, Hualin; Gao, Ying; Chen, Xiaorui; Gao, Jianzhi; Pan, Minghu; Guo, Quanmin

DOI:

[10.1002/sstr.202300230](https://doi.org/10.1002/sstr.202300230)

License:

Creative Commons: Attribution (CC BY)

Document Version

Publisher's PDF, also known as Version of record

Citation for published version (Harvard):

Ding, H, Zhang, X, Li, B, Wang, Y, Xia, C, Zhao, H, Yang, H, Gao, Y, Chen, X, Gao, J, Pan, M & Guo, Q 2023, 'Oriental Growth of Flexible van der Waals Supramolecular Networks', *Small Structures*.
<https://doi.org/10.1002/sstr.202300230>

[Link to publication on Research at Birmingham portal](#)

General rights

Unless a licence is specified above, all rights (including copyright and moral rights) in this document are retained by the authors and/or the copyright holders. The express permission of the copyright holder must be obtained for any use of this material other than for purposes permitted by law.

- Users may freely distribute the URL that is used to identify this publication.
- Users may download and/or print one copy of the publication from the University of Birmingham research portal for the purpose of private study or non-commercial research.
- User may use extracts from the document in line with the concept of 'fair dealing' under the Copyright, Designs and Patents Act 1988 (?)
- Users may not further distribute the material nor use it for the purposes of commercial gain.

Where a licence is displayed above, please note the terms and conditions of the licence govern your use of this document.

When citing, please reference the published version.

Take down policy

While the University of Birmingham exercises care and attention in making items available there are rare occasions when an item has been uploaded in error or has been deemed to be commercially or otherwise sensitive.

If you believe that this is the case for this document, please contact UBIRA@lists.bham.ac.uk providing details and we will remove access to the work immediately and investigate.

Oriental Growth of Flexible van der Waals Supramolecular Networks

Haoxuan Ding, Xin Zhang, Bosheng Li, Yitao Wang, Chunqiu Xia, Haoyu Zhao, Hualin Yang, Ying Gao, Xiaorui Chen, Jianzhi Gao,* Minghu Pan,* and Quanmin Guo*

The capacity for nanopatterning and functionality is a promising facet of supramolecular self-assembly. However, the formation of molecular frameworks entirely dependent on van der Waals (vdW) interactions is infrequently explored. Herein, 2D vdW supramolecular structures are synthesized through the self-assembled cocrystallization of C₆₀ and decanethiol (DT) molecules on Au(111) surface. Notably, the system eliminates the need of functional groups for specific bonding between adjacent units. The conformation C₆₀/DT is delicately manipulated by adjusting molecular coverage and annealing temperature. The absence of directional bonding between C₆₀ and DT molecules facilitates the formation of a variety of stable phases at room temperature (RT), such as 1) porous C₆₀ networks with thiol-filled pores and 2) self-synthesized (C₆₀)_n nanochains with thiol spacers interspersed between the chains are achieved and visualized by scanning tunneling microscopic imaging under RT. This innovative integration of the vdW interaction unveils new avenues for developing supramolecular patterns characterized by their comparatively weak but exceptionally adaptable bonding.

1. Introduction

Supramolecular self-assembly provides an efficient mechanism for creating complex systems maintained through noncovalent bonds.^[1,2] This phenomenon entails spontaneous, self-organized aggregation of discrete or interconnected components.^[3,4] Although the methodology is relatively straightforward, self-assembly predominantly relies on a heuristic approach with an element of trial and error.^[5] Nevertheless, a growing interest is being observed in designing bicomponent self-assembled networks, which precisely orchestrate chemically diverse molecular building blocks within a regular matrix.^[6,7] Such bicomponent structures are anticipated to manifest functions unattainable from their single-component counterparts.^[8]

Additionally, supramolecular self-assembly is increasingly recognized as an efficient approach for examining the interplay between fullerene derivatives and substrates.^[9] A ubiquitous example is bicomponent systems embodying host-guest architectures, where one component constitutes the host frameworks and the other assumes the guest role, filling spaces within the host framework.^[10] In specific scenarios, intrinsically porous building blocks are utilized to generate the host network.^[11] These building blocks exhibit covalent cavities, a property intrinsic to their chemical structure.^[12]

A distinct subclass of host networks with covalent cavities includes 2D surface covalent organic frameworks (2D-sCOFs),^[13] recently deployed for trapping guest C₆₀ molecules.^[14] Alternatively, when forming the host network, the precursor molecule can construct a porous framework through self-assembly on surface, facilitated by strategically placed C₆₀ molecules into the molecular framework, such as hydrogen bonding functional groups^[15] or elongated alkyl chains.^[16]


Nonetheless, certain complex molecular networks comprising binary components cannot be easily classified as host-guest networks, primarily because neither of the two assembling components is able to form a host network to begin with. However, these two components can form a cohosted network through distinct intermolecular interactions, resulting in a cocrystalline arrangement^[17,18] dictated by a defined unit cell^[14] or a random mixture.^[19] The phase transition is explained by the competition between molecule-molecule and molecule surface

H. Ding, B. Li, C. Xia, H. Zhao, H. Yang, Y. Gao, Q. Guo
School of Physics and Astronomy
University of Birmingham
Birmingham B15 2TT, UK
E-mail: q.guo@bham.ac.uk

X. Zhang, J. Gao, M. Pan
School of Physics and Information Technology
Shaanxi Normal University
Xi'an 710119, China
E-mail: jianzhigao@snnu.edu.cn; minghupan@snnu.edu.cn

Y. Wang
School of Physics and Astronomy
University of Nottingham
Nottingham NG7 2RD, UK

X. Chen
School of Mechanical and Material Engineering
Xi'an University
Xi'an 710065, China

 The ORCID identification number(s) for the author(s) of this article can be found under <https://doi.org/10.1002/ssstr.202300230>.

© 2023 The Authors. Small Structures published by Wiley-VCH GmbH. This is an open access article under the terms of the Creative Commons Attribution License, which permits use, distribution and reproduction in any medium, provided the original work is properly cited.

DOI: 10.1002/ssstr.202300230

interactions.^[18] These nonhost–guest bicomponent networks on surfaces are widely studied in ultrahigh vacuum (UHV)^[20] and under ambient conditions;^[21] they can be categorized according to dominant intermolecular interactions in the stabilization of self-assembly on surfaces, such as hydrogen bonding,^[22] halogen bonding,^[23] or metal–ligand coordination.^[24] C₆₀ does not have functional groups; hence, its interaction with other molecules relies on cooperative interactions where the stability of 2D assemblies depends on the simultaneous interaction among many molecules instead of that of the nearest neighbor molecules.^[25–28]

Herein, this study investigates the formation of 2D van der Waals (vdW) supramolecular structures through the self-assembled cocrystallization of decanethiol (DT) and C₆₀ molecules on an Au(111) surface at room temperature (RT). Given the absence of specialized functional groups on either the DT or the C₆₀ molecules, the coexistence of such conformers allows for the creation of intricate supramolecular architectures. However, the practical control of supramolecular nanostructures presents significant challenges. We have explored the C₆₀/DT coassembly with flexible phase transition on Au(111) substrate using high-resolution scanning tunneling microscopy (STM).

As illustrated in **Figure 1**, the DT/Au(111) self-assembled monolayer (SAMs) serves as the molecular template (also can refer to Figure S1, Supporting Information). The adsorption of DT on Au(111) results in the formation of Au–adatom–decanethiolate, the AAD unit.^[29] The AAD unit can be represented as RS–Au–SR (R = CH₃(CH₂)₉).^[30,31] The RS–Au–SR staples form long-range ordered crystalline domains at saturation coverage with a nearest neighbor distance of 0.5 nm. A combined sulfur–gold interaction and the vdW interaction between the alkyl chains

stabilize the ordered thiol monolayer. The alkyl chains tilt about 30° from the surface normal at high coverage. Also, they are found to lie nearly flat on the surface at low coverages.^[32]

Earlier studies on this system unveiled phase-separated C₆₀ and thiols on Au(111) with no signs of a regular mixture.^[33–35] A saturated octanethiol (OT) monolayer^[33] can prevent C₆₀ molecules from reaching the Au(111) substrate except at locations of defects. On a propylthiol monolayer, C₆₀ forms close-packed domains even at 100 K with clear phase-separated domains of C₆₀ and thiol at RT. The relatively short propyl chains do not offer strong enough interactions with C₆₀. Hence, no ordered C₆₀–thiol mixture is observed at any coverage of propylthiol.^[34] Here, we take a different approach, preparing the DT layer with less than the saturation coverage. This approach effectively promotes the trapping of C₆₀ molecules and opens the path to forming cocrystals of C₆₀ and DT. The DT/Au(111) SAMs sample is heated in a UHV chamber to 393 K for 2 h, leading to partial desorption of DT and the emergence of the striped δ phase with a coverage of 0.23 ML (one monolayer is defined as one DT molecule per surface Au atom), wherein each segment comprises a small number of AAD units, as depicted in Figure 1a and Figure S1d, Supporting Information. Subsequently, around 0.045 ML of C₆₀ molecules are deposited onto the DT striped phase monolayer and incorporated into the AAD units via defect sites between staggered DT segments. Due to the favorable C₆₀–C₆₀ and C₆₀–thiol interaction directed self-assembly, the supramolecular C₆₀ framework manifests with thiol-filled pores in Figure 1b. The porous structure transforms into C₆₀ nanochains upon annealing with thiols occupying the space between neighboring C₆₀ chains, as shown in Figure 1c. This research elucidates the

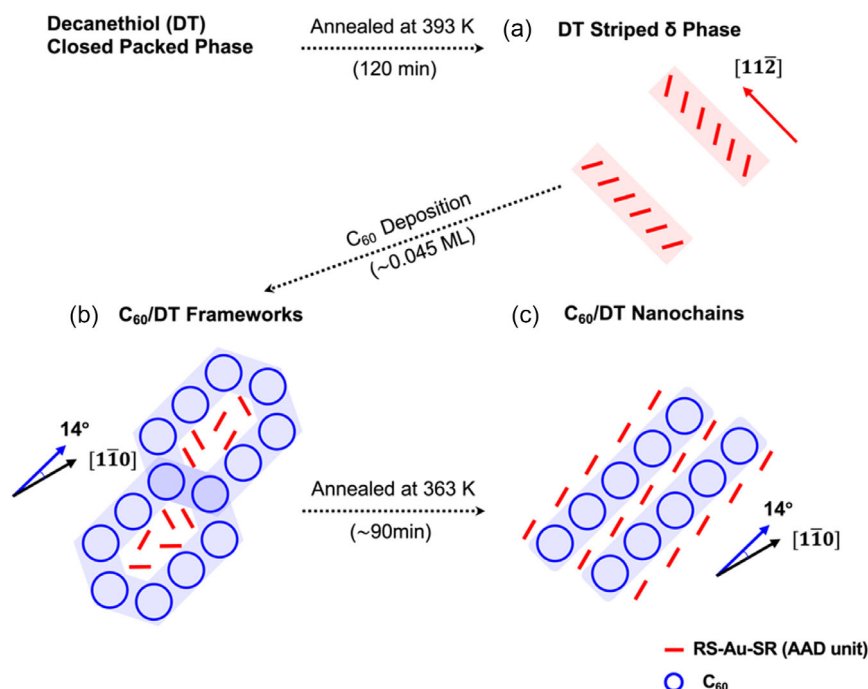


Figure 1. Schematic illustration of the design principle of C₆₀/DT coassembly on surface. a) Schematic of the striped phase consisting of rows of AAD. Each red bar represents the S–Au–S axis, with the alkyl chains not shown for clarity. b) Porous C₆₀ framework with pores filled with AAD. C₆₀ molecules are shown according to the observed STM images, but AAD is shown for illustrative purposes only, as the exact locations of AAD have not been accurately determined. c) C₆₀ nanochain array confined by the aligned AAD units.

competition between equilibrium and metastable phases steered by molecular coverage, molar ratios, and annealing temperature.

2. Results and Discussion

2.1. C₆₀ Dimerization within DT/Au(111) Matrix

Prior research examining the deposition of C₆₀ onto saturated octanethiol (OT) monolayers (0.33 ML) has shown that the full coverage OT monolayer exhibits limited receptivity to C₆₀,^[33] with C₆₀ molecules being incorporated into the OT monolayer through a small number of defect sites^[33] (also refer to Figure S2, Supporting Information). In the current investigation, we remove a fraction of thiol molecules via thermal desorption. The remaining thiols are reorganized into a striped structure. The striped structure consisting of staggered AAD rows offers regular docking sites for C₆₀. An STM image presented in **Figure 2a** shows the formation of a number of C₆₀ islands after deposition of C₆₀ onto DT/Au(111) which is kept at RT.^[31] Contrary to observations of C₆₀ adsorption on bare Au(111),^[36] it is rare to observe close packed C₆₀ molecules in this stage.

Figure 2a suggests that the C₆₀ islands nucleate at some particular sites, presumably defects within the DT layer. Once a nucleus is formed, it expands by capturing more C₆₀ molecules. In contrast to the formation of close packed C₆₀ islands on bare Au(111), hardly any C₆₀ islands are formed from step edges on

the DT/Au(111) surface. This is either due to the steps being heavily passivated by thiols or the diffusion of C₆₀ toward the steps hindered by the AAD rows. Our observations indicate that C₆₀ molecules form C₆₀ dimers and initiate growth from defects within segmented DT rows (refer to Figure S2a, Supporting Information). The C₆₀ molecules are observed to be 0.43 nm taller than the baseline level established by the DT striped phase. DT has an apparent height of 0.18 nm when measured using STM from bare Au(111) substrate. Thus, C₆₀ appears 0.61 nm taller than the Au(111) substrate. This height is consistent with C₆₀ molecules embedded within the DT self-assembled monolayers (SAMs) and directly bonded to the gold substrate,^[37,38] analogous to golf balls in a patch of grass. Upon landing, C₆₀ molecules diffuse over DT until they find a docking site which is usually a defect within the DT layer. At the docking site, the C₆₀ molecule moves downward and becomes directly attached to Au(111). As more and more C₆₀ molecules are added, DT needs to give up some of its territory. This is achieved by moving the alkyl chain from a nearly flat-lying configuration toward the surface normal in junction with lateral movement of DT molecules. The end result is that DT molecules as a whole occupy smaller area on Au(111) after C₆₀ are incorporated. This is equivalent to compression of the DT layer into a higher density phase.^[34] Figure 2e shows a schematic diagram illustrating the relationship between C₆₀ molecules and AAD units in various locations.

Figure 2b illustrates the [1 $\bar{1}0$] and [11 $\bar{2}$] directions of Au(111) as indicated by the blue and green arrows, respectively.

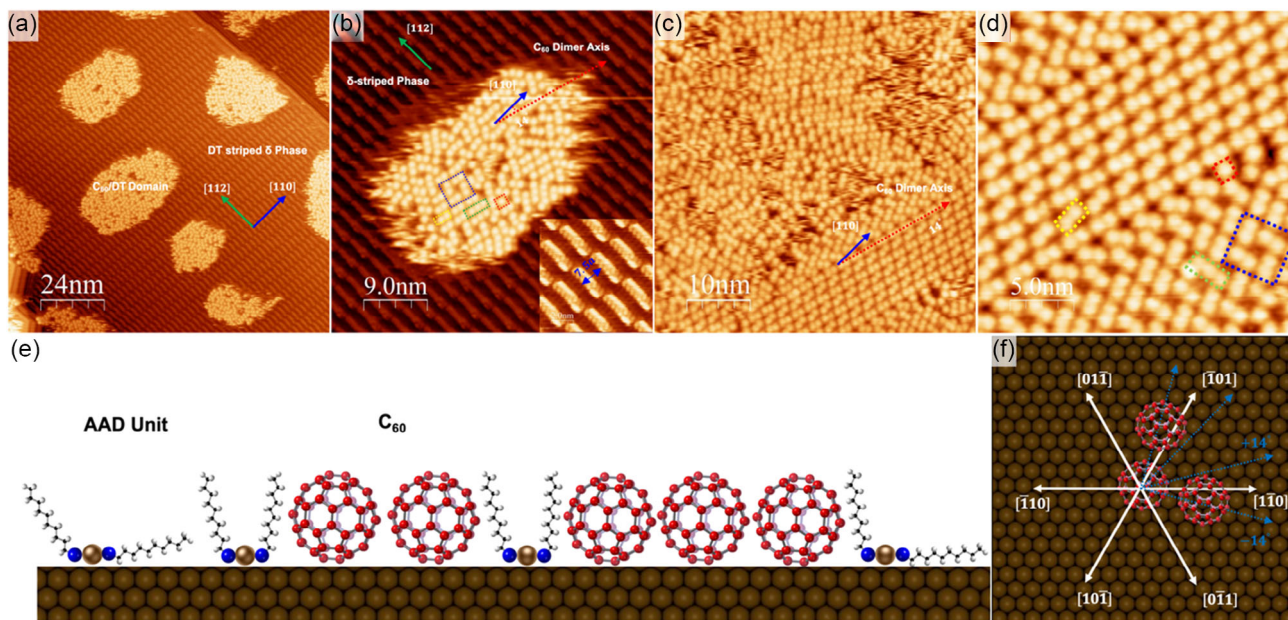


Figure 2. The initial growth of mixed C₆₀/DT islands at RT. a) STM image (120 nm × 120 nm) shows domains of C₆₀/DT coexisting with DT striped δ phase on the Au(111) surface. The green arrow denotes the [11 $\bar{2}$] direction, which also aligns with the DT rows in the δ phase. The blue arrow signifies the [1 $\bar{1}0$] direction, the angle between C₆₀ dimer axis and [1 $\bar{1}0$] direction is 14° ($V_b = 1.5$ V; $I_t = 0.3$ nA). b) High-resolution STM image (45 nm × 45 nm; $V_b = 1.5$ V; $I_t = 0.3$ nA) of top left domain of (a). C₆₀ monomer, dimer, and trimer are delineated by red, yellow, and green rectangles, respectively. A blue rectangle marks the metastable C₆₀ square pore. The inset (10 nm × 10 nm; $V_b = 1.8$ V; $I_t = 0.3$ nA) provides a magnified view of DT striped δ phase. c) STM image of (50 nm × 50 nm; $V_b = -1.8$ V; $I_t = 0.3$ nA) C₆₀ dimer rows is formed after annealing at 323 K for 30 min. d) High-resolution STM image (25 nm × 25 nm; $V_b = -1.5$ V; $I_t = 0.3$ nA) of the bottom right domain of (c). A coexistence C₆₀ monomer, dimer, trimer, and square porous are marked. e) A schematic diagram illustrates the relationship between C₆₀ molecules and the AAD units in various locations on Au(111). f) The dimer axis is 14° on either side of the close packed direction of Au(111). Hence, there are six possible directions. Four of the six possible directions for the C₆₀ dimer axis are illustrated.

The DT rows in the δ phase are found to be parallel to the $[11\bar{2}]$ direction.^[32] Notably, in Figure 2c,d, the C_{60} molecules tend to pair up after the sample was annealed at 323 K for 30 min. The dimer axis is 14° on either side of the $[1\bar{1}0]$ crystal direction. Figure 2f shows there are six such directions. On the bare Au(111) surface, C_{60} can form more than three close packed phases.^[39] One of the close packed phases is known as the R14 phase. The dimer axis is aligned along the same direction as the close packing direction of C_{60} molecules in the R14 phase.^[36,37] The distance between the two C_{60} molecules in each dimer is measured to be 1.00 ± 0.05 nm by using the typical distance between DT molecules as the reference.^[30] This distance is the same as the nearest neighbor distance of C_{60} molecules associated with the R14 phase.

Each C_{60} island in Figure 2a,c is a mixture of C_{60} and DT. Without DT being involved, C_{60} would simply form close packed domains. The high-resolution STM images of a C_{60} /DT domains, as shown in Figure 2b,d, reveal the presence of dimers, trimers, and monomers, with dimers the dominant species. DT fills the gaps between the C_{60} molecules, although the STM cannot locate these DT molecules. This is due to different tunneling conductance, as will be discussed later. One can see that two or more dimers align themselves to form short dimer rows in Figure 2c. However, we only observe short-range order here as the growth process is significantly hindered by kinetics. In an earlier study with C_{60} and octanethiol, long-range order appears at RT.^[35] In order to form a long-range ordered C_{60} /thiol mixture, the initial striped structure of thiol must be broken first. The alkyl chain of DT is longer than that of OT, and thus it presents a higher energy barrier for reorganization. The inset image illustrates the period of the DT striped phase as $7.5a$, where “ a ” represents the nearest neighbor distance for Au atoms. Each striped phase comprises regularly spaced AAD rows, with the distance between two neighboring rows dependent on the coverage.^[32,40]

We can clearly see the locations of individual C_{60} molecules in Figure 2d. However, we are not able to determine the locations of the DT molecules within the C_{60} /DT mixture experimentally. This is most likely due to the significant difference in tunneling conductance.^[41] C_{60} measures ≈ 0.6 nm (apparent height measured with the STM) from the Au(111) substrate. Standing up DT molecules measures < 0.2 nm from Au(111). When C_{60} and DT sit next to each other, the contribution of C_{60} toward the overall tunnel current overshadows that of DT. This is partly due to the finite size of the STM tip. An infinitely narrow STM tip would be required in order to resolve the DT molecules. The individual C_{60} molecules are somewhat unstable and are observed to shift under normal scanning conditions, as indicated by the presence of horizontal streaks surrounding the molecules.

For C_{60} /DT coassembly, the primary building blocks can be categorized into monomer, dimer, and trimer (observable in Figure 2b,d), which are highlighted by red, green, and yellow dot frames, respectively. Although dimers are the preferred structure, the existence of monomers is a direct consequence of kinetic constraint. In Figure 2b,d, one can also see four dimers enclosing a space that DT occupies. This is a primitive porous structure. More porous structures are observed upon thermal annealing and will be presented in the next section.

It is noteworthy that the distance between neighboring C_{60} within the dimer or trimer is 1.00 ± 0.05 nm, thereby indicating close packed alignment along the dimer or trimer axis. Apart from molecules in the dimer, other C_{60} - C_{60} distances are significantly greater than 1.00 nm. In Figure 2f, multiple possibilities for the dimer or trimer axis can be observed, each axis being rotated from the $[1\bar{1}0]$ direction by 14° . All six possible directions of the dimer axis have been observed in C_{60} /DT system.

2.2. Formation of C_{60} /DT Porous Framework

In molecular systems where vdW forces constitute the dominant bonding mechanism, the diversity of achievable structures can be rather constrained. This is due to the tendency of vdW forces to guide the molecules toward a close packed arrangement at the nanoscale.^[34] Hence, control over a binary molecular self-assembly system, solely reliant on vdW forces, presents significant challenges.^[42,43]

In an earlier study, when C_{60} was deposited onto octanethiol/Au(111), spontaneous formation of porous frameworks was observed at RT.^[35] We also observe the formation of porous frameworks when C_{60} is added to DT/Au(111). However, long-range order is poor with DT, and the C_{60} /DT mixture usually exists in a rather disordered state, as shown in Figure 2. The order of the mixture is found to depend on several parameters, including sample temperature, C_{60} /thiol ratio, and the quality of the preprepared thiol/Au(111) sample. To demonstrate the effect of temperature, we show STM images in Figure 3, obtained after thermal annealing a C_{60} /DT mixture to 343 K for 30 min.

Comparing Figure 2c with Figure 3a, one can see clearly that the overall order of the C_{60} /DT mixture has been improved after annealing. There are still a substantial number of C_{60} dimers in Figure 3a, but the dominant structure is now the porous framework. Six, eight, or ten C_{60} molecules can form the pore, leading directly to different pore sizes. The number of AAD inside the pore depends on the pore size. We have not been able to produce a porous framework with a single structure, indicating that the energy difference between the coexisting structures is rather small.

In Figure S3a, Supporting Information, an STM image of a mixed C_{60} /DT layer displays four distinct structures: 1) porous C_{60} /DT frameworks in varying hexagonal shapes, 2) a pure striped phase of DT forming parallel rows, 3) patches of $(C_{60})_7$ clusters, and 4) staggered domains of C_{60} nanochains. If the annealing temperature is further increased, parallel zig-zag rows of C_{60} eventually become the only structural phase. Some C_{60} rows can be seen in Figure 3a. This transition to C_{60} rows is associated with an increased C_{60} /thiol ratio as thiol becomes thermally desorbed.

Figure 3a presents an STM image illustrating the coexistence of hexagonal C_{60} frameworks and C_{60} nanochain structures on the Au(111) surface. White lines outline the relative azimuthal orientations of framework domains I and II. All the C_{60} rows within the C_{60} /DT frameworks are staggered and segmented, with a further 14° clockwise or counterclockwise rotation relative to the $[1\bar{1}0]$ directions of Au(111) (see SI Figure S3b, Supporting Information), aligning with the close-packing direction of C_{60} in the R14 phase.^[36]

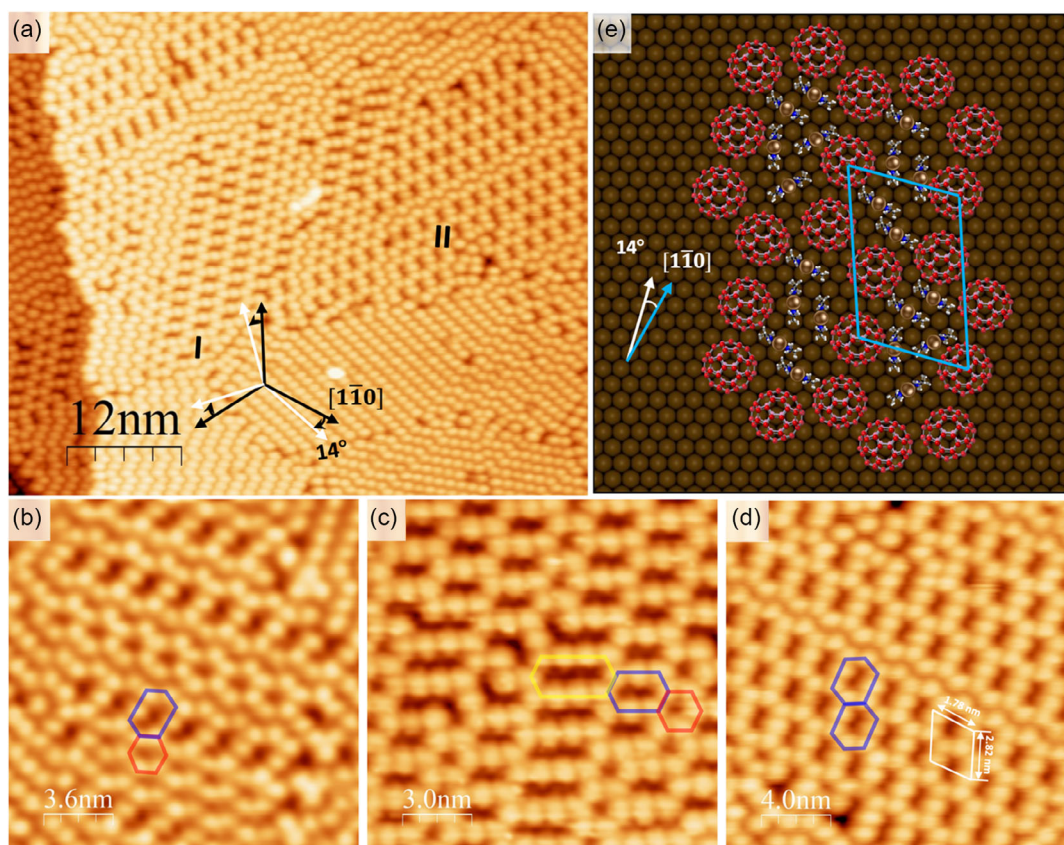


Figure 3. Formation of C_{60} /DT porous frameworks after thermal annealing at 343 K for 30 min. a) An STM image ($60 \text{ nm} \times 50 \text{ nm}$; $V_b = 1.5 \text{ V}$; $I_t = 0.3 \text{ nA}$) illustrating the concurrent existence of the C_{60} /DT frameworks and the zig-zag C_{60} nanochains at RT. Notably, all the segmented C_{60} rows conform to one of the C_{60} closed packed directions. b–d) High-resolution STM images depict three distinct arrangements of C_{60} /DT hexagonal frameworks, marked by red, blue, and yellow hexagons. Tunneling parameters are $V_b = 1.4 \text{ V}$ and $I_t = 0.1 \text{ nA}$ for all STM images. The image sizes are ($18 \text{ nm} \times 18 \text{ nm}$) for (b), ($15 \text{ nm} \times 15 \text{ nm}$) for (c), and ($25 \text{ nm} \times 25 \text{ nm}$) for (d). e) A ball model of the $(C_{60})_8$ porous framework. Each pore is large enough to accommodate five AAD units, although the exact configuration of the five AAD is not yet clear. It visually represents the unit cell illustrated in (d).

The high-resolution STM images in Figure 3b–d display a $(C_{60})_8$ framework (highlighted by a blue hexagon) accompanied by two distinct pore structures: $(C_{60})_6$ (in a red hexagon) and $(C_{60})_{10}$ (in a yellow hexagon). $(C_{60})_8$ is the most abundant on the surface. The coexistence of pores of various sizes indicates that these different sized pores have similar stability. It is not yet understood how to achieve a single-sized pore structure for C_{60} /DT. In our earlier investigation with C_{60} /OT, the self-assembly process seems to be able to self-select pores consisting of six C_{60} molecules.^[35]

To create a structural model of the framework, we embarked on a progressive fine-tuning of the model. Beginning with an initial model derived purely from triangulation, we then filled the RS–Au–SR staples into the pores. The adsorption of the RS–Au–SR alkanethiol staples on Au(111) is well documented.^[44] Filling the pores with DT must conform to the established principle that the Au adatom occupies the bridge site with the RS–Au–SR axis perpendicular to the bridge. The shortest distance between two alkyl chains is around 0.5 nm .^[30] It is also vital that the alkyl chains maintain a reasonable distance from the carbon atoms within the C_{60} cage. The framework is laterally shifted above Au(111) multiple times until the optimal fit is achieved.

Figure 3e presents an optimized structural model for the $(C_{60})_8$ framework. The arrangement of C_{60} molecules in the model matches quite well with what is observed in STM images. We have no reliable information about the locations of the AAD from STM; a trial-and-error approach is taken. The thiol molecules inside the pore interact with each other as well as with C_{60} . Thiol molecules inside the pore are not in an equivalent bonding environment. However, to optimize the thiol– C_{60} interaction, the alkyl chains need to be oriented nearly perpendicular to the substrate. According to the structural model of Figure 3e, each pore contains five AAD units. The local coverage of DT inside each pore is around 0.33 ML , corresponding to the coverage of the standing up phase of thiol on Au(111).^[30] Hence, the alkyl chains assume an almost vertical orientation inside the pores and are perpendicular to the Au surface. According to the model in Figure 3e, if we place five AAD units inside the pore, the C_{60} coverage in the framework is 0.045 ML , and the DT coverage is 0.15 mL , resulting in a C_{60} /DT ratio of 3:10. Both the coverages for C_{60} and DT are scaled to the atomic density of surface Au atoms. Consequently, the framework composition is $(C_{60})_3(DT)_{10}$. Also, the molar ratio of C_{60} /OT frameworks is 4:14 in our previous study.^[35] When compared to 4:14

and 3:10, they exhibit comparable magnitudes. This correspondence serves as evidence that our proposed model aligns effectively with the appropriate level. Additionally, the initial coverage of DT in the δ phase also stands at 0.23 ML,^[31] reaffirming a reduction in the overall thiol coverage. During the deposition of C_{60} or the subsequent thermal annealing process, some thiol molecules may have desorbed, as we do not observe mass migration of DT to areas surrounding the framework (see Figure S3, Supporting Information).

A noteworthy attribute of the C_{60} /DT framework is that its structure does not solely rely on nearest neighbor interactions. Instead, collective interactions among a large number of molecules dictate the stable structure transition. This is a marked deviation from hydrogen-bonded frameworks^[7] or MOFs,^[45] where nearest neighbor bonding predominantly determines the final structure of the framework.

2.3. Evolution of C_{60} /DT Nanochains

In accordance with prior research, thermal annealing has been recognized as an effective method to modulate molecular

adsorption configurations and assembly processes.^[46–48] For the C_{60} /DT system, thermal treatment causes preferential removal of DT through thermal desorption. This then changes the C_{60} /DT ratio resulting in the change of structures. It is noteworthy that the desorption temperature of C_{60} exceeds that of DT by more than 200 K. Upon annealing the sample at 363 K for 30 min, we observed C_{60} zig-zag nanochains, as depicted in **Figure 4a**. The formation of the C_{60} rows results from further reduction of the thiol coverage due to thermal desorption. C_{60} molecules are close packed along the row. There is a space between two neighboring rows, and DT occupies this space. This C_{60} /DT row phase is similar to the C_{60} /OT rows formed under similar experimental conditions.^[49] However, it is interesting to note that the C_{60} /DT nanochains are considerably longer than the C_{60} rows formed with OT after thermal treatment (Figure S5, Supporting Information). The direction of the C_{60} chains is plus or minus 14° from the $[1\bar{1}0]$ directions of Au(111), the same as the direction of the dimer axis.

Upon further heating the sample to 363 K for 1 h, STM images, as presented in Figure 4b, reveal the disappearance of the staggered C_{60} rows. Now, long-range ordered C_{60} nanochains

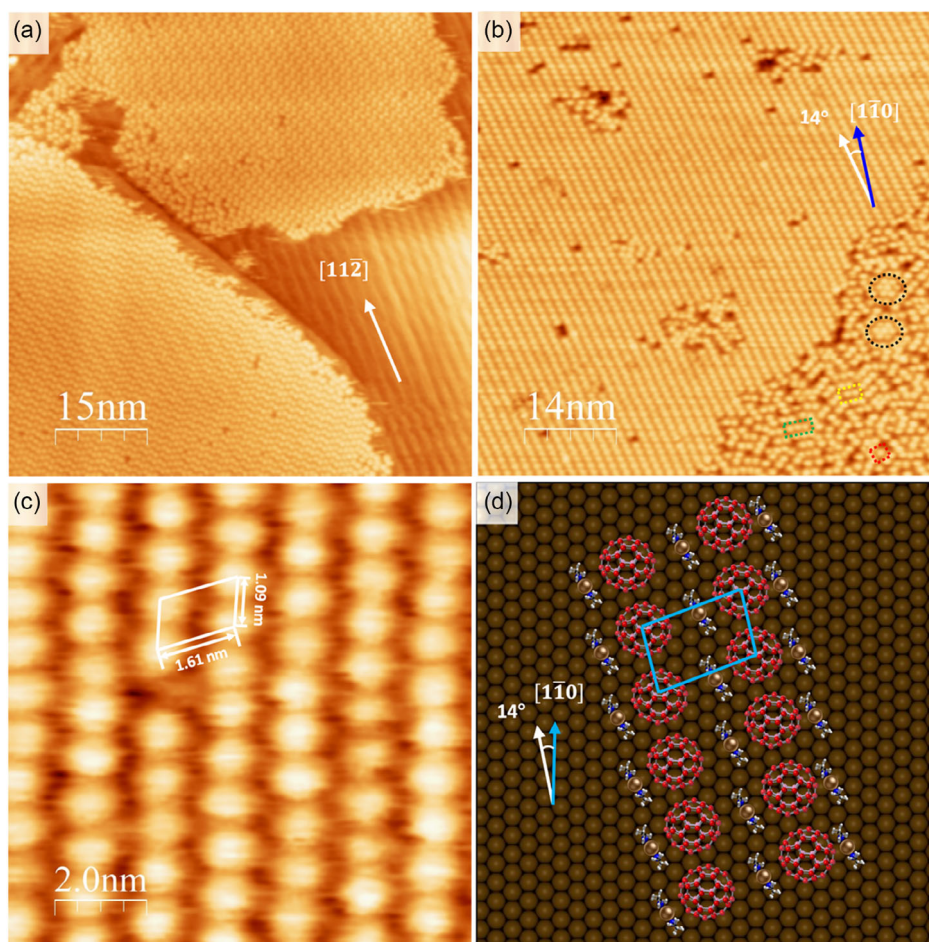


Figure 4. Long-range ordered C_{60} nanochain structure. a) STM image ($75\text{ nm} \times 75\text{ nm}$; $V_b = -1.6\text{ V}$; $I_t = 0.15\text{ nA}$) depicts zig-zag C_{60} rows after annealing at 363 K for 30 min. b) STM image ($70\text{ nm} \times 70\text{ nm}$; $V_b = -1.0\text{ V}$; $I_t = 0.2\text{ nA}$) shows the long C_{60} nanochains after 90 min annealing. The lower right corner shows C_{60} molecules that have not yet formed regular rows. b) A high-resolution STM image ($10\text{ nm} \times 10\text{ nm}$; $V_b = 1.0\text{ V}$; $I_t = 0.3\text{ nA}$) illustrating a C_{60} nanochain with a unit cell. d) The optimized ball model provides a visual representation of the unit cell illustrated in (c).

emerge, following the growth direction of closely packed C_{60} . From these observations, we deduce that the shape of individual building blocks plays a pivotal role in the bottom-up self-assembly of nanostructured materials.^[50] Even a simple change in shape, as from OT to DT, can significantly influence the assembly process due to the modified length of the orientational alkyl chains.

The symmetry of the C_{60} nanochain structure is reduced to twofold symmetry.^[49] A white quadrilateral highlights the unit cell in a high-resolution STM image (Figure 4c). Employing a modeling approach similar to the previously mentioned, we can propose the structural model of segments with a C_{60} -(DT)₂ composition, as illustrated in Figure 4d. The respective coverages of C_{60} and DT molecules are 0.045 and 0.09 ML. In the long-chain direction, there is no spacing between adjacent molecules, allowing RS–Au–SR staples to fill the space between two C_{60} chains.

Similar to the forming process of the C_{60} framework, starting with the square pore structure, the local coverage of DT can be reduced by gently heating the sample. This will keep the local coverage of C_{60} constant and only change the molar ratio between DT and C_{60} . As the C_{60} /DT ratio increases, we observe a gradual transition from a porous C_{60} network to C_{60} chains. All the structures in this system follow an orientational growth along the direction 14° from $[1\bar{1}0]$ direction.

Subsequent thermal annealing prompts a transition from a staggered C_{60} nanochain to a straight one. The rearrangement of molecules during the annealing process signifies the importance of thermodynamics in shaping the final nanostructure. The final C_{60} nanochain is characterized by a higher level of order and reduced molecular freedom, indicative of a lower total energy state. This suggests that the straight C_{60} nanochain is thermodynamically more stable than the staggered arrangement.

3. Conclusion

In conclusion, we have successfully engineered a 2D C_{60} /DT porous molecular framework and extensive nanochain structures on Au(111) surface at room temperature. This bicomponent molecular self-assembly is primarily governed by a cooperative vdW interaction, eliminating the need for specific bonding via functional groups among neighboring molecules. By controlling the molecular coverage and annealing temperature, we can synthesize flexible bicomponent molecular structures, leading to orientational growth.^[50] This approach enriches our fundamental understanding of vdW coassembly on surfaces and offers a promising strategy for creating complex functional nanostructures.^[51,52] This work will likely significantly impact the future design and synthesis of molecular nanostructures/nanomaterials, offering enhanced control over their structures and properties.

4. Experimental Section

The experiments were conducted at RT utilizing an Omicron variable temperature scanning tunneling microscope (VT-STM) in an UHV environment, maintaining a base pressure on the order of 10^{-10} mbar. The Au(111) substrate was a 300 nm-thick film, prepared by depositing gold atoms onto a graphite substrate in a UHV chamber. The substrate

underwent numerous cycles of Ar^+ sputtering and annealing in UHV for surface cleaning, using Ar^+ ions with an energy of 1.5 keV. The resultant vacancy defects created by sputtering at RT were eliminated by annealing above 700 K, producing the standard herringbone reconstructed Au(111) surface. The STM was calibrated using the single atomic layer Au steps and the parameters of the herringbone reconstructed surface unit cell.

A self-assembled DT monolayer was formed on Au(111) by submerging the sample in a 1 mM DT/ethanol solution for 24 h. The sample was subsequently placed into the UHV chamber, which underwent thermal annealing at 393 K for 2 h. This annealing process triggered partial desorption of the DT, forming a striped δ phase. C_{60} molecules were then deposited onto the sample featuring the striped phase of DT at RT. The C_{60} and DT molecules mixed through molecular diffusion, resulting in the emergence of an array of bicomponent structures.

STM images were obtained using electrochemically polished tungsten tips. The lateral distance measured was subject to an uncertainty of ± 0.05 nm. However, this does not imply that features separated by 0.05 nm could be readily determined from a single measurement. Given the periodic nature of the structure being measured, distances spanning multiple unit cell dimensions were measured. Through multiple measurements of this kind, we achieved lateral distance values with an ultimate precision of ± 0.05 nm. The long-range order of the DT striped phase, C_{60} closed-packed structures, and $(C_{60})_7$ clusters, in conjunction with the measured distance and lattice direction, were used in determining the adsorption sites of individual C_{60} molecules. STM images were recorded in a constant current mode under RT and analyzed with WSxM software.^[53]

Supporting Information

Supporting Information is available from the Wiley Online Library or from the author.

Acknowledgements

This work was financially supported by the European Commission (Project Code D-SPA 734578), National Natural Science Foundation of China (Project Codes 21972083 and 22102129), the Fundamental Research Funds for the Central Universities (GK202102008), the Support Program for top-notch young talents in Shaanxi Province (1511000066), and the China Postdoctoral Science Foundation (2021M692615, 2022T150528).

Conflict of Interest

The authors declare no conflict of interest.

Author Contributions

H.X.D., X.Z., and B.S.L. contributed equally to this work. Q.M.G., J.Z.G., and M.H.P. conceived and designed the experiment. H.X.D., X.Z., B.S.L., and C.Q.X. grew the samples and performed the STM experiments. H.X.D. and Q.M.G. analyzed the data and wrote the manuscript with inputs from all other authors. Correspondence should be addressed to J.Z.G., M.H.P., and Q.M.G.

Data Availability Statement

The data that support the findings of this study are available from the corresponding author upon reasonable request.

Keywords

decaneithiol, fullerenes, scanning tunneling microscopy, self-assembly, supramolecular frameworks, van der Waals

Received: July 5, 2023
Revised: August 29, 2023
Published online:

- [1] N. Champness, in *Supramolecular Chemistry on Surfaces: 2D Networks and 2D Structures*, Wiley-VCH, Weinheim **2022**.
- [2] K. Kuhnke, C. Große, P. Merino, K. Kern, *Chem. Rev.* **2017**, *117*, 5174.
- [3] L. Verstraete, S. D. Feyter, *Chem. Soc. Rev.* **2021**, *50*, 5884.
- [4] J. V. Barth, *Annu. Rev. Phys. Chem.* **2007**, *58*, 375.
- [5] E. Geagea, F. Palmino, F. Cherioux, *Chemistry* **2022**, *4*, 796.
- [6] P. A. Staniec, L. M. A. Perdigão, A. Saywell, N. R. Champness, P. H. Beton, *ChemPhysChem* **2007**, *8*, 2177.
- [7] J. A. Theobald, N. S. Oxtoby, M. A. Phillips, N. R. Champness, P. H. Beton, *Nature* **2003**, *424*, 1029.
- [8] B. O. Okesola, A. Mata, *Chem. Soc. Rev.* **2018**, *47*, 3721.
- [9] J. Geng, Q. Zeng, C. Wang, *Nano Res.* **2019**, *12*, 1509.
- [10] J. Teyssandier, S. D. Feyter, K. S. Mali, *Chem. Commun.* **2016**, *52*, 11465.
- [11] E. Mena-Osteritz, P. Bäuerle, *Adv. Mater.* **2006**, *18*, 447.
- [12] G. Pan, J. Liu, H. Zhang, L. Wan, Q. Zheng, C. Bai, *Angew. Chem.* **2003**, *115*, 2853.
- [13] M. O. Blunt, J. C. Russell, N. R. Champness, P. H. Beton, *Chem. Commun.* **2010**, *46*, 7157.
- [14] D. Cui, M. Ebrahimi, F. Rosei, J. M. Macleod, *J. Am. Chem. Soc.* **2017**, *139*, 16732.
- [15] M. O. Blunt, J. C. Russell, M. D. C. Gimenez-Lopez, N. Taleb, X. Lin, M. Schröder, N. R. Champness, P. H. Beton, *Nat. Chem.* **2011**, *3*, 74.
- [16] G.-B. Pan, X.-H. Cheng, S. Höger, W. Freyland, *J. Am. Chem. Soc.* **2006**, *128*, 4218.
- [17] M. Pivetta, M. Blüm, F. Patthey, W. Schneider, *Angew. Chem. Int. Ed.* **2008**, *47*, 1076.
- [18] G. Copie, F. Cleri, Y. Makoudi, C. Krzeminski, M. Berthe, F. Cherioux, F. Palmino, B. Grandidier, *Phys. Rev. Lett.* **2014**, *114*, 066101.
- [19] Y. Zhang, Y. Zhang, G. Li, J. Lu, X. Lin, Y. Tan, X. Feng, S. Du, K. Müllen, H.-J. Gao, *J. Chem. Phys.* **2015**, *142*, 101911.
- [20] W. Xiao, D. Passerone, P. Ruffieux, K. Ait-Mansour, O. Gröning, E. Tosatti, J. S. Siegel, R. Fasel, *J. Am. Chem. Soc.* **2008**, *130*, 4767.
- [21] X. Qiu, C. Wang, Q. Zeng, B. Xu, S. Yin, H. Wang, S. Xu, C. Bai, *J. Am. Chem. Soc.* **2000**, *122*, 5550.
- [22] X. Zhang, H. Ding, S. Yang, H. Yang, X. Yang, B. Li, X. Xing, Y. Sun, G. Gu, X. Chen, J. Gao, M. Pan, L. Chi, Q. Guo, *Small* **2023**, *19*, 2207111.
- [23] Q.-N. Zheng, X.-H. Liu, T. Chen, H.-J. Yan, T. Cook, D. Wang, P. J. Stang, L.-J. Wan, *J. Am. Chem. Soc.* **2015**, *137*, 6128.
- [24] D. Ćija, J. I. Urgel, A. C. Papageorgiou, S. Joshi, W. Auwärter, A. P. Seitsonen, S. Klyatskaya, M. Ruben, S. Fischer, S. Vijayaraghavan, J. Reichert, J. V. Barth, *Proc. Natl. Acad. Sci.* **2013**, *110*, 6678.
- [25] F. Sedona, M. D. Marino, A. Basagni, L. Colazzo, M. Sambri, *J. Phys. Chem. C* **2014**, *118*, 1587.
- [26] H. L. Zhang, W. Chen, L. Chen, H. Huang, X. S. Wang, J. Yuhara, A. T. S. Wee, *Small* **2007**, *3*, 2015.
- [27] J. A. Smerdon, R. B. Rankin, J. P. Greeley, N. P. Guisinger, J. R. Guest, *ACS Nano* **2013**, *7*, 3086.
- [28] W. Jin, D. B. Dougherty, W. G. Cullen, S. Robey, J. E. Reutt-Robey, *Langmuir* **2009**, *25*, 9857.
- [29] P. Maksymovych, D. C. Sorescu, J. T. Yates, *Phys. Rev. Lett.* **2006**, *97*, 146103.
- [30] F. Li, L. Tang, W. Zhou, Q. Guo, *J. Am. Chem. Soc.* **2010**, *132*, 13059.
- [31] G. E. Poirier, *Langmuir* **1999**, *15*, 1167.
- [32] Q. Guo, F. Li, *Phys. Chem. Chem. Phys.* **2014**, *16*, 19074.
- [33] F. Li, L. Tang, W. Zhou, Q. Guo, *J. Phys. Chem. C* **2009**, *113*, 17899.
- [34] J. Gao, J. Gao, C. Yan, M. R. Fard, D. Kaya, G. Zhu, Q. Guo, *J. Phys. Chem. C* **2016**, *120*, 25481.
- [35] X. Zhang, X. Fan, G. Zhu, Y. Wang, H. Ding, H. Lin, Y. Li, Q. Li, J. Gao, M. Pan, Q. Guo, *J. Phys. Chem. C* **2020**, *124*, 12589.
- [36] G. Schull, R. Berndt, *Phys. Rev. Lett.* **2007**, *99*, 226105.
- [37] L. Tang, Y. Xie, Q. Guo, *J. Chem. Phys.* **2011**, *135*, 114702.
- [38] L. Tang, Q. Guo, *Phys. Chem. Chem. Phys.* **2012**, *14*, 3323.
- [39] J. A. Gardener, G. A. D. Briggs, M. R. Castell, *Phys. Rev. B* **2009**, *80*, 235434.
- [40] X. Zhang, J. Gao, X. Fan, Y. Wang, H. Ding, X. Qin, S. Jiang, T. Zhao, G. Zhu, H. Lu, Z. Yang, H. Lin, Q. Li, L. Chi, M. Pan, Q. Guo, *J. Phys. Chem. C* **2019**, *123*, 25228.
- [41] H. Ding, J. Gao, H. Zhao, C. Xia, M. Grose, F.-S. Li, Q. Guo, *J. Phys. Chem. C* **2020**, *124*, 25892.
- [42] S. B. Lei, C. Wang, S. X. Yin, C. L. Bai, *J. Phys. Chem. B* **2001**, *105*, 12272.
- [43] S. B. Lei, S. X. Yin, C. Wang, L. J. Wan, C. L. Bai, *Chem. Mater.* **2002**, *14*, 2837.
- [44] P. Maksymovych, O. Voznyy, D. B. Dougherty, D. C. Sorescu, J. T. Yates, *Prog. Surf. Sci.* **2010**, *85*, 206.
- [45] N. Lin, A. Langner, S. L. Tait, C. Rajadurai, M. Ruben, K. Kern, *Chem. Commun.* **2007**, *46*, 4860.
- [46] Y. L. Huang, W. Chen, H. Li, J. Ma, J. Pflaum, A. T. S. Wee, *Small* **2010**, *6*, 70.
- [47] L. Feng, T. Wang, Z. Tao, J. Huang, G. Li, Q. Xu, S. L. Tait, J. Zhu, *ACS Nano* **2019**, *13*, 10603.
- [48] C. Li, Q. Zeng, Y. Liu, L. Wan, C. Wang, C. Wang, C. Bai, *ChemPhysChem* **2003**, *4*, 857.
- [49] X. Zhang, H. Ding, X. Chen, H. Lin, Q. Li, J. Gao, M. Pan, Q. Guo, *Nanoscale* **2022**, *14*, 1333.
- [50] L. Guo, Y. Wang, D. Kaya, R. E. Palmer, G. Chen, Q. Guo, *Nano Lett.* **2018**, *18*, 5257.
- [51] L. Guo, Y. Wang, D. Kaya, Z. Wang, M. Zhang, Q. Guo, *Appl. Surf. Sci.* **2021**, *538*, 148142.
- [52] Y. Wang, L. Guo, Q. Guo, *J. Phys. Chem. C* **2019**, *123*, 7776.
- [53] I. Horcas, R. Fernández, J. M. Gómez-Rodríguez, J. Colchero, J. Gómez-Herrero, A. M. Baro, *Rev. Sci. Instrum.* **2007**, *78*, 013705.